Received: 21 October 2019 | Revised: 4 June 2020 | Accepted: 16 June 2020

DOI: 10.1002/we.2550

WILEY

RESEARCH ARTICLE

Robust structural control of an underactuated floating wind turbine

Yangming Zhang | Xiaowei Zhao | Xing Wei

School of Engineering, University of Warwick, Coventry, UK

Correspondence
Xiaowei Zhao, School of Engineering, University of Warwick, Coventry CV4 7AL, UK.
Email: xiaowei.zhao@warwick.ac.uk

Funding information
Engineering and Physical Sciences Research Council, Grant/Award Number: EP/R015120/1

Abstract

This paper investigates the dynamic modeling and robust control of an underactuated floating wind turbine for vibration suppression. The offshore wind turbine is equipped with a tuned mass damper on the floating platform. The Lagrange's equation is employed to establish the limited degree-of-freedom dynamic model. A novel disturbance observer-based hierarchical sliding mode control system is developed for mitigating loads of the underactuated floating wind turbine. In the proposed control scheme, two prescribed performance nonlinear disturbance observers are developed to estimate and counteract unknown disturbances, where the load induced by wave is considered as a mismatched disturbance while the load caused by wind is treated as a matched disturbance. The hierarchical sliding mode controller regulates the states of such an underactuated nonlinear system. In particular, the first-order sliding mode differentiator is used to avoid the tedious analytic computation in the sliding mode control design. The stability of the whole closed-loop system is rigorously analyzed, and some sufficient conditions are derived to guarantee the convergence of the states for the considered system. Numerical simulations deployed on both the design model and the National Renewable Energy Laboratory 5-MW wind turbine model are provided, which demonstrate great effectiveness and strong robustness of the proposed control scheme.

KEYWORDS

vibration control, wind turbine, hierarchical sliding mode control, mismatched disturbance, underactuated nonlinear systems

1 | INTRODUCTION

Wind power has drawn more and more attention in recent years,[1-3] with an increasing number of offshore wind turbines installed. This is because offshore wind resources are of higher quality than the onshore case.[4,5] According to types of foundations, offshore wind turbines can be roughly categorized as fixed-bottom ones and floating ones. The fixed-bottom turbines are often placed in water with depth up to 60 m. The floating wind turbines are usually installed in the ocean from 60 m to upwards of 900 m or beyond. Moreover, the floating structures are more economical in deep water regions and much less dependent on the seabed conditions than the fixed-bottom ones. However, the floating wind turbines are susceptible to the adverse effect of the loads induced by wind and wave, which would lead to the considerable vibration fatigue damages on the

wind turbine structures. Therefore, vibration suppression of floating wind turbines becomes a significant topical area of research in order to reduce their maintenance costs and increase their life cycle.

During the past decade, many efforts have been made to suppress the vibrations of wind turbine by reducing tilt motions of the tower top or the floating platform. The representative methodologies mainly include passive, semi-active, and active structural control. Passive structural control systems do not require the power supply with constant parameters, such as tuned mass damper (TMD).[6] An advantage of TMD-based control is that it does not disturb the power generation while its disadvantage is that it needs extra mass. This disadvantage can be minimized if an existing turbine component can serve as the mass component, such as the reservoir in a hydrostatic wind turbine.[7] By comparison with passive structural control systems, semi-active structural control systems have time-varying parameters that can be tuned during operation, such as semi-active TMD[8] and magnetorheological dampers.[9] Unlike passive control systems, active structural control designs use an actuator to produce a control force on the mass and structure; its advantage is that a greater impact on the platform pitch or the tower bend angle can be achieved.[10] This paper focuses on active control. Active structural control designs with TMDs installed in the nacelle were considered for vibration suppression of the floating offshore wind turbines,[11] where the H_∞ multivariable loop-shaping method was used to design an active structural controller. To simplify the control architecture, a generalized H_∞ approach was proposed for a TMD on the platform.[12] The TMD-based floating wind turbine was regarded as a simplified linear model with small angle approximations in other studies.[11,12] However, the floating wind turbine is an underactuated nonlinear coupled system with both mismatched and matched disturbances. Therefore, it is useful to develop an advanced controller to handle the nonlinearity effectively.

Sliding mode control is a popular robust nonlinear control technique due to its strong robustness against parameter variations and external disturbances.[13] Over the past two decades, sliding mode control has been successfully applied to many practical underactuated physical systems, such as inverted-pendulum systems,[14] planar vehicles,[15] mobile robots,[16] underwater vehicles,[17] and hypersonic vehicles.[18] Different from the existing sliding mode control structures,[14-18] Wang et al.[19] proposed a hierarchical sliding mode control scheme, which can be accommodated to most second-order underactuated systems. With the aid of the proposed hierarchical sliding mode control,[19] an adaptive controller was developed to stabilize four states of the spherical robot.[20] However, the above papers do not consider adverse effects of mismatched disturbances. Although Xu et al.[21] considered this issue, their sliding mode control approach was only effective for diminishing disturbance rejections. The TMD-based floating offshore wind turbine is a more complex underactuated nonlinear coupled system with both matched and mismatched disturbances. To the authors' knowledge, there is no results reported to design a sliding mode controller for such a system.

Motivated by the aforementioned discussions, a more complete nonlinear dynamic model is established for the TMD-based floating offshore wind turbine system without linearization. A disturbance observer-based adaptive hierarchical sliding mode control algorithm is proposed to regulate both actuated and unactuated degrees of freedom for this nonlinear coupled system with nondiminishing disturbances. Two disturbance observers are independently designed to estimate both matched and mismatched disturbances respectively, where the estimated accuracy of each disturbance observer can be adjusted by only one parameter. The established model is divided into two subsystems; several sliding variables are constructed to develop a hierarchical sliding mode controller for such a system. To reduce the computing burden, the first-order sliding mode differentiator is used to estimate the derivative of the designed disturbance observer. Finally, strong robustness and excellent control performance of the proposed control algorithm are shown by the simulation tests.

2 | SYSTEM DESCRIPTION AND PROBLEM FORMULATION

In this section, we briefly introduce the floating wind turbine with the TMD configuration and establish an underactuated nonlinear coupled dynamic model.

2.1 | A TMD-based National Renewable Energy Laboratory 5-MW floating wind turbine

We start with a description of the structure of a TMD-based floating wind turbine as depicted in Figure 1, which is primarily composed of a rotor–nacelle assembly (RNA), a tower, an ITI Energy platform, a mooring system, and a TMD. The nacelle houses a few mechanical and electrical components such as the drivetrain, generator, and converters. The tower is mounted on the ITI Energy barge platform. The rigid barge platform is moored by eight catenary lines to alleviate drifting. The TMD is placed on the barge platform. As shown in Figure 1, the platform has six motion degree-of-freedoms (DOFs), which includes three translational DOFs (i.e., surge, sway, and heave) and three rotational DOFs (i.e., roll, pitch, and yaw), where *X*, *Y*, and *Z*represent the set of orthogonal axes with their origin denoted by O. The *X*-axis designates the nominal downwind direction, the *XY*-plane represents the mean sea level, and the *Z*-axis points upward opposite to gravity along the centerline of the unbending tower when the platform is undisplaced. In this study, the National Renewable Energy Laboratory (NREL) 5-MW baseline wind turbine[22,23] is used for the analysis and control design. The physical parameters of the NREL 5MW baseline wind turbine and the ITI barge platform are listed in Table 1.[24]

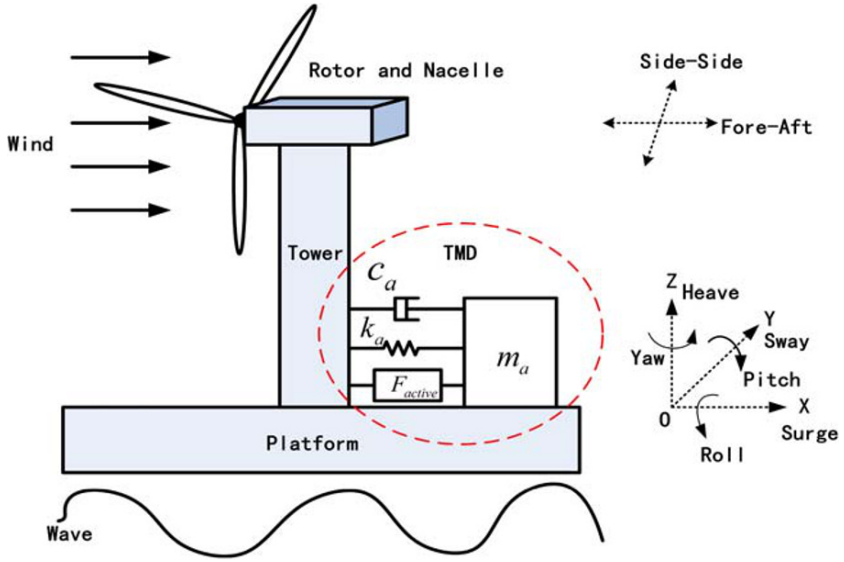

FIGURE 1 Schematic of a floating offshore wind turbine with a tuned mass damper (TMD) configuration in the platform

TABLE 1 Parameters of the National Renewable Energy Laboratory 5-WM wind baseline turbine and the ITI barge platform

Description	Value
Rating power	5 MW
Rotor orientation	Upwind
Baseline control	Variable speed, collective pitch
Rotor diameter	126 m
Hub height	90 m
Cut-in, rated, cut-out wind speed	3 m/s, 11.4 m/s, 25 m/s
Cut-in, rated rotor speed	6.9 rpm, 12.1 rpm
Platform size (L×W×H)	40×40×10 m
Rotor mass	110 000 kg
Nacelle Mass	240 000 kg
Tower Mass	347 460 kg
Platform Mass	5 452 000 kg
Anchor Depth	150 m

2.2 | Dynamic modeling of a TMD-based floating wind turbine

Note that the fore–aft direction has the largest loading from winds and waves. It is obvious that the highest fatigue damage on the tower is from this direction. Three most-relevant DOFs originated from the tower first bend mode, the platform pitch motion, and the TMD motion. For modeling purposes, the tower is regarded as an inverted pendulum with the structural damping and stiffness, which are modeled as a rotary damper and rotary spring at the base of the rigid body. The effect imposed on the barge platform from the mooring lines and the hydrodynamics is considered as a linear spring and a linear damper. Therefore, the kinetic and potential energies of the TMD-based floating offshore wind turbine can be expressed as

$$T_{op} = \frac{1}{2} I_{tp} \dot{\theta}_t^2 + \frac{1}{2} I_{bp} \dot{\theta}_p^2 + \frac{1}{2} m_a \dot{x}_a^2, \tag{1}$$

$$\begin{aligned} V_{op} = {} & \frac{1}{2} k_{tp} (\theta_t - \theta_p)^2 + \frac{1}{2} (C_{hs} + C_{ml}) \theta_p^2 + m_t g L_t \cos\theta_t - m_p g L_p \cos\theta_p \\ & + \frac{1}{2} k_a (h_c \sin\theta_t - x_a)^2 - m_a g x_a \sin\theta_p, \end{aligned} \tag{2}$$

where T_{op} is the total kinetic energy, V_{op} is the total potential energy, θ_t is the bend angle of the pendulum tower from the Z-axis, θ_p is the pitch angle of the platform, x_a is the longitudinal displacement of the TMD, I_{tp} represents the inertia moment of the tower & RNA, I_{bp} is the platform pitch inertia, m_a is the mass of the TMD, k_{tp} is the equivalent pitch restoring coefficient of the tower and RNA, C_{hs} is the hydrostatic pitch restoring coefficient, C_{ml} denotes the linearized pitch restoring coefficient from mooring lines, m_t is the total mass of the tower and RNA, g is the gravitational acceleration, L_t is the distance from the mass center of the tower and RNA to the reference point O, m_p is the mass of the platform, L_p is the distance from the mass center of the platform to the reference point O, k_a denotes the stiffness of the TMD, and h_c is the distance from the mass center of the TMD to the reference point O. The nonconservative forces acting on the tower first bend mode, the platform pitch motion, and the TMD displacement can be described by

$$f_{L_p} = -A_{rad}\ddot{\theta}_p - (B_{rad} + B_{vis})\dot{\theta}_p + d_{tp}(\dot{\theta}_t - \dot{\theta}_p) + M_w, \tag{3}$$

$$f_{L_t} = -d_{tp}(\dot{\theta}_t - \dot{\theta}_p) + F_a L_{hh} - c_a h_c(h_c\dot{\theta}_t - \dot{x}_a) - h_c F_{active}, \tag{4}$$

$$f_{L_a} = c_a(h_c\dot{\theta}_t - \dot{x}_a) + F_{active}, \tag{5}$$

where A_{rad} is the added pitch inertia associated with hydrodynamic radiation, B_{rad} is the pitch damping coefficient with respect to hydrodynamic radiation, B_{vis} is the linearized pitch damping coefficient with regard to hydrodynamic viscous drag, d_{tp} represents the equivalent pitch damping coefficient of the tower & RNA, M_w denotes the total wave-excitation pitch moment from diffraction applied at the reference point O, F_a is the aerodynamic rotor thrust acting on the hub, and L_{hh} is the height of the hub, c_a is the damping coefficient of the TMD, and F_{active} is the force delivered by the active control system. According to the Lagrange's equation approach, we have

$$\frac{d}{dt}\left(\frac{\partial L_{op}}{\partial \dot{\theta}_p}\right) - \frac{\partial L_{op}}{\partial \theta_p} = f_{L_p}, \tag{6}$$

$$\frac{d}{dt}\left(\frac{\partial L_{op}}{\partial \dot{\theta}_t}\right) - \frac{\partial L_{op}}{\partial \theta_t} = f_{L_t}, \tag{7}$$

$$\frac{d}{dt}\left(\frac{\partial L_{op}}{\partial \dot{x}_a}\right) - \frac{\partial L_{op}}{\partial x_a} = f_{L_a}, \tag{8}$$

where L_{op}=T_{op}−V_{op}. By virtue of (1)–(8), the overall vibration dynamic model of the TMD-based floating offshore wind turbine can be expressed as

$$\begin{aligned}(A_{rad} + I_{bp})\ddot{\theta}_p = &-(C_{hs} + C_{ml} + k_{tp})\theta_p - (B_{rad} + B_{vis} + d_{tp})\dot{\theta}_p + d_{tp}\dot{\theta}_t \\ &+ k_{tp}\theta_t + m_a g x_a \cos\theta_p - L_p g m_p \sin\theta_p + M_w,\end{aligned} \tag{9}$$

$$\begin{aligned}I_{tp}\ddot{\theta}_t = \; &d_{tp}\dot{\theta}_p - (d_{tp} + c_a h_c^2)\dot{\theta}_t + c_a h_c \dot{x}_a + k_{tp}\theta_p - k_{tp}\theta_t \\ &- k_a h_c^2 \cos\theta_t \sin\theta_t + k_a h_c x_a \cos\theta_t + L_t g m_t \sin\theta_t \\ &- F_{active} h_c + F_a L_{hh},\end{aligned} \tag{10}$$

$$m_a\ddot{x}_a = -c_a\dot{x}_a + c_a h_c\dot{\theta}_t - k_a x_a + m_a g \sin\theta_p + k_a h_c \sin\theta_t + F_{active}. \tag{11}$$

For control purposes, we define state variables as $x_1 = \theta_p$, $x_2 = \dot{\theta}_p$, x_3=θ_t, $x_4 = \dot{\theta}_t$, $x_5 = x_a$, $x_6 = \dot{x}_a$, and rewrite the whole system (9)–(11) as

$$\begin{aligned}\dot{x}_1 &= x_2, \\ \dot{x}_2 &= -a_{p1}x_1 - a_{p2}x_2 + a_{p3}x_3 + a_{p4}x_4 + a_{p5}x_5\cos x_1 - a_{p6}\sin x_1 + d_w,\end{aligned} \tag{12}$$

$$\begin{aligned}\dot{x}_3 &= x_4, \\ \dot{x}_4 &= a_{t1}x_1 + a_{t2}x_2 - a_{t3}x_3 - a_{t4}x_4 - a_{t5}\cos x_3 \sin x_3 + a_{t6}x_6 + a_{t7}\sin x_3 \\ &\quad + a_{t8}x_5\cos x_3 - b_{t1}u + d_z,\end{aligned} \tag{13}$$

$$\begin{aligned}\dot{x}_5 &= x_6, \\ \dot{x}_6 &= a_{m1}\sin x_1 + a_{m2}\sin x_3 - a_{m3}x_5 + a_{m4}x_4 - a_{m5}x_6 + b_{m1}u,\end{aligned} \tag{14}$$

where

$$a_{p1}=\frac{C_{hs}+C_{ml}+k_{tp}}{A_{rad}+I_{bp}},\quad a_{p2}=\frac{B_{rad}+B_{vis}+d_{tp}}{A_{rad}+I_{bp}},\quad a_{p3}=\frac{k_{tp}}{A_{rad}+I_{bp}},\quad a_{p4}=\frac{d_{tp}}{A_{rad}+I_{bp}},$$
$$a_{p5}=\frac{m_a g}{A_{rad}+I_{bp}},\quad a_{p6}=\frac{L_p g m_p}{A_{rad}+I_{bp}},\quad a_{t1}=a_{t3}=\frac{k_{tp}}{I_{tp}},\quad a_{t2}=\frac{d_{tp}}{I_{tp}},\quad a_{t4}=\frac{d_{tp}+c_a h_c^2}{I_{tp}},$$
$$a_{t5}=\frac{k_a h_c^2}{I_{tp}},\quad a_{t6}=\frac{c_a h_c}{I_{tp}},\quad a_{t7}=\frac{L_t g m_t}{I_{tp}},\quad a_{t8}=\frac{k_a h_c}{I_{tp}},\quad b_{t1}=\frac{h_c}{I_{tp}},\quad a_{m1}=g,\quad a_{m2}=\frac{k_a h_c}{m_a},$$
$$a_{m3}=\frac{k_a}{m_a},\quad a_{m4}=\frac{c_a h_c}{m_a},\quad a_{m5}=\frac{c_a}{m_a},\quad b_{m1}=\frac{1}{m_a},\quad u=F_{active},\quad d_w=\frac{M_w}{A_{rad}+I_{bp}},\quad d_z=\frac{L_{hh}F_a}{I_{tp}}.$$

Note that x_5 and x_6 are the displacement and velocity of the TMD. The TMD is placed on the platform; its displacement and velocity are necessary to be restricted in scope due to the limited space of the platform (as shown in Table 1). Note that d_w and d_z are the external excitations from the effects of wave and wind. Assume that d_w and d_z are the bounded disturbances, which are required to satisfy the conditions $|d_w| \le D_w$ and $|d_z| \le D_z$, where D_w and D_z are positive constants. u is the control input. The control objective is to design a single controller u to guarantee the convergence of x_1, x_2, x_3, and x_4 for the underactuated floating offshore wind turbine in the presence of both mismatched and matched disturbances.

Lemma 1. [25]: The first-order sliding mode differentiator is given by

$$\begin{aligned}\dot{\zeta}_0 &= \eta_0 = -\epsilon_0|\zeta_0 - h(t)|^{\frac{1}{2}}\text{sign}(\zeta_0 - h(t)) + \zeta_1,\\ \dot{\zeta}_1 &= -\epsilon_1 \text{sign}(\zeta_1 - \eta_0),\end{aligned} \tag{15}$$

where ζ_0, ζ_1, and η_0 are the states of the system (15), ϵ_0 and ϵ_1 are the design parameters of such a sliding mode differentiator, and $h(t)$ is a known function. Then, η_0 can approach the differential term $\dot{h}(t)$ with arbitrary accuracy if the initial deviations $\zeta_0 - h(t_0)$ and $\eta_0 - \dot{h}(t_0)$ are bounded.

Lemma 2. [26]: Consider the continuous and differentiable bounded function $\varpi(t)$, $\forall t \in [t_0, t_1]$, if $\varpi(t)$ satisfies $|\varpi(t)| \le D$, then $\dot{\varpi}(t)$ is bounded, where D is a positive constant.

3 | MAIN RESULTS

From (12)–(14), it is clear to see that the floating offshore wind turbine with the TMD configuration is a complex underactuated nonlinear coupled system with both matched and mismatched disturbances. The conventional sliding mode control cannot be directly applied in such a system due to the existence of underactuated strong coupled features and mismatched disturbances. In this section, we will present both the controller design and the stability analysis.

3.1 | Disturbance observer-based hierarchical sliding mode control design

Note that the nondiminishing disturbances cause big difficulty in the design of the sliding mode control system, especially for the presence of mismatched disturbances. To deal with both matched and mismatched disturbances, two prescribed performance observers are separately developed to estimate their values for disturbance rejections. According to the assumptions $|d_w| \le D_w$ and $d_z \le D_z$, it is obtained from Lemma 2 that both $\dot{d}_w$ and $\dot{d}_z$ are bounded. It is reasonable to assume that $\dot{d}_w \le \overline{D}_w$ and $\dot{d}_z \le \overline{D}_z$, where $\overline{D}_w > 0$ and $\overline{D}_z > 0$. Define

$$\begin{aligned}\vartheta_p &= [-a_{p1}, a_{p3}, a_{p4}, a_{p5}, -a_{p6}]^T,\\ f_p &= [x_1, x_3, x_4, x_5\cos x_1, \sin x_1]^T,\\ \varphi_p &= [\varphi_{p1}, \varphi_{p3}, \varphi_{p4}, \varphi_{p5}, \varphi_{p6}]^T.\end{aligned}$$

Then, it is indicated from (12) that

$$\dot{x}_2 = -a_{p2}x_2 + \vartheta_p^T f_p + d_w. \tag{16}$$

Using (16), we construct the disturbance observer $\hat{d}_w$ to estimate the mismatched diturbance d_w in the following form:

$$\hat{d}_w = \varepsilon_p + \beta_p x_2 + \varphi_p^T \vartheta_p, \tag{17}$$

$$\dot{\varepsilon}_p = -\beta_p \varepsilon_p + \beta_p a_{p2} x_2 - \beta_p^2 x_2, \tag{18}$$

$$\dot{\varphi}_p = -\beta_p \varphi_p - \beta_p f_p, \tag{19}$$

where $\beta_p > 0$.

Lemma 3. By applying the disturbance observer (17)–(19), the estimation error $\tilde{d}_w = d_w - \hat{d}_w$ satisfies

$$\lim_{t\to\infty} \tilde{d}_w = \Delta_1, \tag{20}$$

where Δ_1 can converge to an arbitrarily small constant.

Proof. Choose the following Lyapunov-like function candidate

$$V_w = \frac{1}{2}\tilde{d}_w^2. \tag{21}$$

The time derivative of V_w can be calculated as

$$\dot{V}_w = \tilde{d}_w(\dot{d}_w - \dot{\hat{d}}_w) \le -\tilde{d}_w \dot{\hat{d}}_w + \overline{D}_w|\tilde{d}_w|. \tag{22}$$

Substituting (16)–(19) into (22), we have

$$\begin{aligned} \dot{V}_w &\le -\tilde{d}_w \dot{\hat{d}}_w + \overline{D}_w|\tilde{d}_w| \\ &= -\beta_p \tilde{d}_w(d_w - \varepsilon_p - \beta_p x_2 - \varphi_p^T \vartheta_p) + \overline{D}_w|\tilde{d}_w| \\ &= -\beta_p \tilde{d}_w(d_w - \hat{d}_w) + \overline{D}_w|\tilde{d}_w| \\ &= -\beta_p \tilde{d}_w^2 + \overline{D}_w|\tilde{d}_w|. \end{aligned} \tag{23}$$

Applying Young's inequality,[27] based on (23) we have

$$\begin{aligned} \dot{V}_w &\le -\beta_p \tilde{d}_w^2 + \overline{D}_w|\tilde{d}| \\ &= -\frac{\beta_p}{2}\tilde{d}_w^2 + \left(-\frac{\beta_p}{2}\tilde{d}_w^2 + \overline{D}_w|\tilde{d}_w|\right) \\ &\le -\frac{\beta_p}{2}\tilde{d}_w^2 + \frac{\overline{D}_w^2}{2\beta_p}. \end{aligned} \tag{24}$$

From (24), we have

$$\tilde{d}_w^2 \le [d_w(0) - \hat{d}_w(0)]^2 e^{-\beta_p t} + \frac{\overline{D}_w^2}{\beta_p^2}. \tag{25}$$

According to (25), we derive

$$\lim_{t\to\infty} |\tilde{d}_w| \le \frac{\overline{D}_w}{\beta_p}. \tag{26}$$

Therefore, the estimation error $\tilde{d}_w$ can converge to any arbitrarily small constant by appropriately selecting one adjustable parameter. In other words, we can choose a large β_p to ensure the excellent estimation performance.

Similarly, a disturbance observer with prescribed performance is designed to estimate the matched disturbance d_z for disturbance rejections. Define

$$\begin{aligned}\vartheta_z &= [a_{t1}, a_{t2}, -a_{t3}, -a_{t5}, a_{t6}, a_{t7}, a_{t8}]^T,\\ f_z &= [x_1, x_2, x_3, \cos x_3 \sin x_3, x_6, \sin x_3, x_5 \cos x_3]^T,\\ \varphi_z &= [\varphi_{z1}, \varphi_{z2}, \varphi_{z3}, \varphi_{z5}, \varphi_{z6}, \varphi_{z7}, \varphi_{z8}]^T.\end{aligned}$$

Then, we rewrite (13) as

$$\dot{x}_4 = -a_{t4}x_4 + \vartheta_z^T f_z - b_{t1}u + d_z. \tag{27}$$

In this case, the disturbance observer can be given by

$$\hat{d}_z = \varepsilon_z + \beta_z x_4 + \varphi_z^T \vartheta_z, \tag{28}$$

$$\dot{\varepsilon}_z = -\beta_z \varepsilon_z + \beta_z a_{t4} x_4 + \beta_z b_{t1} u - \beta_z^2 x_4, \tag{29}$$

$$\dot{\varphi}_z = -\beta_z \varphi_z - \beta_z f_z, \tag{30}$$

where $\beta_z > 0$.

Lemma 4. The disturbance observer (28)–(30) is designed to guarantee that the estimation error $\tilde{d}_z = d_z - \hat{d}_z$ satisfies

$$\lim_{t\to\infty} \tilde{d}_z = \Delta_2, \tag{31}$$

where Δ_2 can converge to an arbitrarily small constant.

Proof. Consider the following Lyapunov-like function candidate

$$V_z = \frac{1}{2}\tilde{d}_z^2. \tag{32}$$

With the similar derivation process as the proof of Lemma 3, the time derivative of V_z can be computed from (27)–(30), which can be expressed as

$$\dot{V}_w \le -\frac{\beta_z}{2}\tilde{d}_z^2 + \frac{\overline{D}_z^2}{2\beta_z}. \tag{33}$$

By virtue of (33), we have

$$\tilde{d}_z^2 \le [d_z(0) - \hat{d}_z(0)]^2 e^{-\beta_z t} + \frac{\overline{D}_z^2}{\beta_z^2}, \tag{34}$$

which implies

$$\lim_{t\to\infty} |\tilde{d}_z| \le \frac{\overline{D}_z}{\beta_z}. \tag{35}$$

Therefore, we can select a large β_z such that the estimation error $\tilde{d}_z$ converges to any arbitrarily small constant.

As a matter of fact, if both the mismatched and matched disturbances like most reported literatures[28,29] satisfy the conditions $\lim_{t\to\infty} \dot{d}_w = 0$ and $\lim_{t\to\infty} \dot{d}_z = 0$, it is indicated from (26) and (35) that the disturbance observers $\hat{d}_w$ and $\hat{d}_z$ can track the disturbances d_w and d_z of the considered system asymptotically, respectively. It means $\lim_{t\to\infty} \tilde{d}_w = 0$ and $\lim_{t\to\infty} \tilde{d}_z = 0$.

According to the property of the considered system (12) and (13), we split the overall system into two subsystems, where one is (x_1, x_2, x_3, x_4)-subsystem given by (12)–(13) and the other is (x_3, x_4)-subsystem described by (13). It is important for us to construct proper sliding variables to regulate the states of two subsystems for vibration suppression. We define the errors

$$e_1 = x_1, \tag{36}$$

$$e_2 = x_2, \tag{37}$$

$$e_3 = -a_{p1}x_1 - a_{p2}x_2 + a_{p3}x_3 + a_{p4}x_4 + a_{p5}x_5\cos x_1 - a_{p6}\sin x_1 + \hat{d}_w, \tag{38}$$

$$e_4 = x_3,, \tag{39}$$

$$e_5 = x_4. \tag{40}$$

The sliding variable of the (x_1, x_2, x_3, x_4)-subsystem is selected as

$$s_1 = c_1e_1 + c_2e_2 + e_3, \tag{41}$$

where c_1 and c_2 are positive constants. The time derivative of s_1 is given by

$$\begin{aligned}\dot{s}_1 &= c_1\dot{e}_1 + c_2\dot{e}_2 + \dot{e}_3\\ &= c_1\dot{x}_1 + c_2\dot{x}_2 - a_{p1}x_2 - a_{p2}\dot{x}_2 + a_{p3}x_4 + a_{p4}\dot{x}_4 + a_{p5}(x_6\cos x_1 - x_5x_2\sin x_1)\\ &\quad - a_{p6}x_2\cos x_1 + \dot{\hat{d}}_w.\end{aligned} \tag{42}$$

Substituting (12) and (13) into (42) yields

$$\begin{aligned}\dot{s}_1 = {} & (c_1 - a_{p1})x_2 + (c_2 - a_{p2})(-a_{p1}x_1 - a_{p2}x_2 + a_{p3}x_3 + a_{p4}x_4 + a_{p5}x_5\cos x_1 - a_{p6}\sin x_1\\ & + d_w) + a_{p3}x_4 + a_{p5}x_6\cos x_1 - a_{p5}x_5x_2\sin x_1 - a_{p6}x_2\cos x_1 + \dot{\hat{d}}_w + a_{p4}(a_{t1}x_1 + a_{t2}x_2\\ & - a_{t3}x_3 - a_{t4}x_4 - a_{t5}\cos x_3\sin x_3 + a_{t6}x_6 + a_{t7}\sin x_3 + a_{t8}x_5\cos x_3 - b_{t1}u + d_z).\end{aligned} \tag{43}$$

Then, we have

$$\begin{aligned}\dot{s}_1 = {} & \ell_1x_1 + \ell_2x_2 + \ell_3x_3 + \ell_4x_4 + \ell_5x_5 + \ell_6x_6 - (c_2 - a_{p2})a_{p6}\sin x_1 + (c_2 - a_{p2})d_w + \dot{\hat{d}}_w\\ & - a_{p4}a_{t5}\cos x_3\sin x_3 + a_{p4}a_{t7}\sin x_3 - a_{p4}b_{t1}u + a_{p4}d_z,\end{aligned} \tag{44}$$

where

$$\begin{aligned}\ell_1 &= a_{p4}a_{t1} - (c_2 - a_{p2})a_{p1},\\ \ell_2 &= c_1 - a_{p1} - (c_2 - a_{p2})a_{p2} - a_{p5}x_5\sin x_1 - a_{p6}\cos x_1 + a_{p4}a_{t2},\\ \ell_3 &= (c_2 - a_{p2})a_{p3} - a_{p4}a_{t3},\\ \ell_4 &= (c_2 - a_{p2})a_{p4} + a_{p3} - a_{p4}a_{t4},\\ \ell_5 &= (c_2 - a_{p2})a_{p5}\cos x_1 + a_{p4}a_{t8}\cos x_3\\ \ell_6 &= a_{p5}\cos x_1 + a_{p4}a_{t6}.\end{aligned}$$

Let $\dot{s} = 0$. The equivalent controller of the (x_1, x_2, x_3, x_4)-subsystem can be written as

$$\begin{aligned}u_{1eq} = {} & \frac{1}{a_{p4}b_{t1}}[\ell_1x_1 + \ell_2x_2 + \ell_3x_3 + \ell_4x_4 + \ell_5x_5 + \ell_6x_6 - (c_2 - a_{p2})a_{p6}\sin x_1 + (c_2 - a_{p2})d_w\\ & + \dot{\hat{d}}_w - a_{p4}a_{t5}\cos x_3\sin x_3 + a_{p4}a_{t7}\sin x_3 + a_{p4}d_z],\end{aligned} \tag{45}$$

Note that the controller (45) cannot be used in practice. It is necessary for us to replace the disturbances d_w and d_z with their estimations $\hat{d}_w$ and $\hat{d}_z$, respectively. Thus, we obtain

$$\begin{aligned} u_{1eq} = \ & \frac{1}{a_{p4}b_{t1}}[\ell_1 x_1 + \ell_2 x_2 + \ell_3 x_3 + \ell_4 x_4 + \ell_5 x_5 + \ell_6 x_6 - (c_2 - a_{p2})a_{p6}\sin x_1 + (c_2 - a_{p2})\hat{d}_w \\ & + \dot{\hat{d}}_w - a_{p4}a_{t5}\cos x_3 \sin x_3 + a_{p4}a_{t7}\sin x_3 + a_{p4}\hat{d}_z]. \end{aligned} \tag{46}$$

To avoid the tedious analytic computation of the disturbance observer $\dot{\hat{d}}_w$, the first-order sliding mode differentiator is introduced to estimate $\dot{\hat{d}}_w$. Applying Lemma 1, the first-order sliding mode differentiator can be given by

$$\begin{aligned} \dot{\zeta}_0 &= \eta_0 = -\epsilon_0|\zeta_0 - \hat{d}_w|^{\frac{1}{2}}\text{sign}(\zeta_0 - \hat{d}_w) + \zeta_1, \\ \dot{\zeta}_1 &= -\epsilon_1 \text{sign}(\zeta_1 - \eta_0), \end{aligned} \tag{47}$$

where ζ_0, ζ_1, and η_0 are the states of the system (47) and ϵ_0 and ϵ_1 are positive constants. By virtue of Lemma 1 and (47), we obtain

$$\dot{\hat{d}}_w = \eta_0 + \Delta_3, \tag{48}$$

where Δ_3 is an estimation error of the first-order sliding mode differentiator. It implies from Lemma 1 that $|\Delta_3| \le \overline{\Delta}_3$ with $\overline{\Delta}_3 > 0$. Replacing $\dot{\hat{d}}_w$ with η_0, the equivalent controller of the (x_1, x_2, x_3, x_4)-subsystem can be expressed as

$$\begin{aligned} u_{1eq} = \ & \frac{1}{a_{p4}b_{t1}}[\ell_1 x_1 + \ell_2 x_2 + \ell_3 x_3 + \ell_4 x_4 + \ell_5 x_5 + \ell_6 x_6 - (c_2 - a_{p2})a_{p6}\sin x_1 + (c_2 - a_{p2})\hat{d}_w \\ & + \eta_0 - a_{p4}a_{t5}\cos x_3 \sin x_3 + a_{p4}a_{t7}\sin x_3 + a_{p4}\hat{d}_z]. \end{aligned} \tag{49}$$

The sliding variable of the (x_3, x_4)-subsystem can be chosen as

$$s_2 = c_3 e_4 + e_5, \tag{50}$$

where c_3 is positive constant. The time derivative of s_2 can be computed as

$$\begin{aligned} \dot{s}_2 \ &= c_3\dot{e}_4 + \dot{e}_5 \\ &= c_3 x_4 + \dot{x}_4. \end{aligned} \tag{51}$$

Substituting (13) into the above expression, one gets

$$\begin{aligned} \dot{s}_2 = \ & c_3 x_4 + a_{t1}x_1 + a_{t2}x_2 - a_{t3}x_3 - a_{t4}x_4 - a_{t5}\cos x_3 \sin x_3 + a_{t6}x_6 + a_{t7}\sin x_3 \\ & + a_{t8}x_5 \cos x_3 - b_{t1}u + d_z. \end{aligned} \tag{52}$$

Let $\dot{s}_2 = 0$. The equivalent controller of the (x_3, x_4)-subsystem is described as

$$\begin{aligned} u_{2eq} = \ & \frac{1}{b_{t1}}(c_3 x_4 + a_{t1}x_1 + a_{t2}x_2 - a_{t3}x_3 - a_{t4}x_4 - a_{t5}\cos x_3 \sin x_3 + a_{t6}x_6 + a_{t7}\sin x_3 \\ & + a_{t8}x_5 \cos x_3 + \hat{d}_z). \end{aligned} \tag{53}$$

Note that only one control input can be used to control four state variables. This means that we need to use one control input to ensure two sliding surfaces can be reached (i.e., $s_1 = 0$ and $s_2 = 0$). The conventional sliding mode control method cannot be used for this underactuded nonlinear coupled system. To achieve this goal, a second-layer sliding variable is developed as

$$s = \alpha_1 s_1 + \alpha_2 s_2, \tag{54}$$

where α_1 and α_2 are the sliding mode parameters, which satisfy $\alpha_1 > 0$ and $\alpha_2 > 0$. According to the variable structure theory, the switching control part is required to be designed to ensure the states can reach and thereafter stay on the sliding surface. Thus, the complete controller must include some portion of the switching control part, which can be expressed as

$$u = u_{1eq} + u_{2eq} + u_{sw}, \tag{55}$$

where u_{sw} is the switching term of the sliding mode controller, which can be given by

$$u_{sw} = -\frac{\alpha_2}{\alpha_1 a_{p4} + \alpha_2} u_{1eq} - \frac{\alpha_1 a_{p4}}{\alpha_1 a_{p4} + \alpha_2} u_{2eq} + \frac{\varrho \text{sign}(s)}{(\alpha_1 a_{p4} + \alpha_2) b_{t1}} + \frac{\lambda s}{(\alpha_1 a_{p4} + \alpha_2) b_{t1}}, \tag{56}$$

where ϱ and λ are positive design parameters, which will be given later. Substituting (56) into (55) gives

$$u = \frac{\alpha_1 a_{p4}}{\alpha_1 a_{p4} + \alpha_2} u_{1eq} + \frac{\alpha_2}{\alpha_1 a_{p4} + \alpha_2} u_{2eq} + \frac{\varrho \text{sign}(s)}{(\alpha_1 a_{p4} + \alpha_2) b_{t1}} + \frac{\lambda s}{(\alpha_1 a_{p4} + \alpha_2) b_{t1}}. \tag{57}$$

To reduce the chattering, in practice, some smoothing functions such as $\frac{s}{|s|+\sigma}$ and $\tanh(s)$ are introduced to replace the discontinuous sign function in the sliding mode controller (57), where σ is a small positive constant.

3.2 | Stability analysis

The following theorem presents the design procedure and analysis of the proposed disturbance observer-based hierarchical sliding mode controller for the TMD-based floating offshore wind turbine (9)–(11) in the consideration of both mismatched and matched disturbances with the nonlinear disturbance observers and the sliding mode control technique.

Theorem 1. Consider the TMD-based floating offshore wind turbine system (9)–(11) with both mismatched and matched disturbances. Under the nonlinear disturbance observers given by (17)–(19) and (28)–(30), if the sliding variables are defined in (41), (50), and (54), then the disturbance observer-based hierarchical sliding mode controller (57) guarantees the convergence of x_1, x_2, x_3, and x_4, where both x_1 and x_2 converge to an arbitrarily small value.

Proof. Consider the Lyapunov function candidate

$$V = \frac{1}{2} s^2. \tag{58}$$

With (54), the time derivative of V can be computed as

$$\dot{V} = s(\alpha_1 \dot{s}_1 + \alpha_2 \dot{s}_2). \tag{59}$$

Substituting (44) and (52) into (59), we have

$$\begin{aligned} \dot{V} &= \alpha_1 s \dot{s}_1 + \alpha_2 s \dot{s}_2 \\ &= \alpha_1 s[\ell_1 x_1 + \ell_2 x_2 + \ell_3 x_3 + \ell_4 x_4 + \ell_5 x_5 + \ell_6 x_6 - (c_2 - a_{p2}) a_{p6} \sin x_1 + (c_2 - a_{p2}) d_w + \dot{\tilde{d}}_w \\ &\quad - a_{p4} a_{t5} \cos x_3 \sin x_3 + a_{p4} a_{t7} \sin x_3 - a_{p4} b_{t1} u + a_{p4} d_z] + \alpha_2 s(c_3 x_4 + a_{t1} x_1 + a_{t2} x_2 - a_{t3} x_3 \\ &\quad - a_{t4} x_4 - a_{t5} \cos x_3 \sin x_3 + a_{t6} x_6 + a_{t7} \sin x_3 + a_{t8} x_5 \cos x_3 - b_{t1} u + d_z). \end{aligned} \tag{60}$$

Rearranging (60), we derive

$$\begin{aligned} \dot{V} = \; & \alpha_1 s[\ell_1 x_1 + \ell_2 x_2 + \ell_3 x_3 + \ell_4 x_4 + \ell_5 x_5 + \ell_6 x_6 - (c_2 - a_{p2}) a_{p6} \sin x_1 + (c_2 - a_{p2}) d_w + \dot{\tilde{d}}_w \\ & - a_{p4} a_{t5} \cos x_3 \sin x_3 + a_{p4} a_{t7} \sin x_3 + a_{p4} d_z] + \alpha_2 s(c_3 x_4 + a_{t1} x_1 + a_{t2} x_2 - a_{t3} x_3 - a_{t4} x_4 \\ & - a_{t5} \cos x_3 \sin x_3 + a_{t6} x_6 + a_{t7} \sin x_3 + a_{t8} x_5 \cos x_3 + d_z) - s(\alpha_1 a_{p4} b_{t1} + \alpha_2 b_{t1}) u. \end{aligned} \tag{61}$$

Inserting (48), (49), (53), and (57) into (61), we have

$$\begin{aligned} \dot{V} = \; & \alpha_1 s(c_2 - a_{p2})(d_w - \hat{d}_w) + \alpha_1 s(\dot{\tilde{d}}_w - \eta_0) + (\alpha_1 s a_{p4} + \alpha_2 s)(d_z - \hat{d}_z) - \varrho |s| - \lambda s^2 \\ = \; & \alpha_1 s(c_2 - a_{p2}) \tilde{d}_w + \alpha_1 s \Delta_3 + (\alpha_1 a_{p4} + \alpha_2) s \tilde{d}_z - \varrho |s| - \lambda s^2 \\ = \; & s[\alpha_1 (c_2 - a_{p2}) \tilde{d}_w + \alpha_1 \Delta_3 + (\alpha_1 a_{p4} + \alpha_2) \tilde{d}_z] - \varrho |s| - \lambda s^2. \end{aligned} \tag{62}$$

Let $\psi = \alpha_1(c_2 - a_{p2})\tilde{d}_w + \alpha_1\Delta_3 + (\alpha_1 a_{p4} + \alpha_2)\tilde{d}_z$. Next, it is essential for us to prove the boundedness of ψ. Note that $|\Delta_3| \le \overline{\Delta}_3$ from (48). From Lemmas 3 and 4, it implies from the limit definition that both $\tilde{d}_w$ and $\tilde{d}_z$ are bounded. Hence, it is reasonable to assume $|\psi| \le D$.

$$\begin{aligned} \dot{V} \le & -(\varrho - D)|s| - \lambda s^2 \\ = & -\rho|s| - \lambda s^2, \end{aligned} \tag{63}$$

where $\rho = \varrho - D > 0$. Integrating both sides of (63), we have

$$\int_0^t \dot{V} d\tau \le \int_0^t -\rho|s| - \lambda s^2 d\tau, \tag{64}$$

which indicates

$$\begin{aligned} V(t) = & \frac{1}{2}s^2 \\ & \le V(0) - \int_0^\infty (\rho|s| + \lambda s^2) d\tau \\ & \le V(0) < \infty. \end{aligned} \tag{65}$$

From (65), we have $s \in L_\infty$. By virtue of (63), we obtain

$$\begin{aligned} \dot{V} = & s\dot{s} \\ & \le -\rho|s| - \lambda s^2 < \infty. \end{aligned} \tag{66}$$

It is concluded from (66) that $\dot{s} \in L_\infty$. According to Barbalat's lemma, we have $\lim_{t\to\infty} s = 0$. From (50), we get $s_2 = c_3 x_3 + x_4$. Note that x_3 and x_4 represent the angular displacement and velocity of the tower, respectively. Thus, we have $s_2 \in L_\infty$. The time derivative of s_2 is $\dot{s}_2 = c_3 x_4 + \dot{x}_4$, where $\dot{x}_4$ is the angular acceleration of the tower. Hence, this indicates that $\dot{s}_2 \in L_\infty$. By virtue of (54), we obtain $s_1 \in L_\infty$ and $\dot{s}_1 \in L_\infty$ due to $s \in L_\infty$ and $\dot{s} \in L_\infty$. It is noted that the stability of the system does not depend on the parameters α_1 and α_2. It is reasonable to define two different sliding variables as follows:

$$s_g = \alpha_{1g} s_1 + \alpha_2 s_2, \quad s_h = \alpha_{1h} s_1 + \alpha_2 s_2, \tag{67}$$

where α_{1g} and α_{1h} are positive constants with $\alpha_{1g} \neq \alpha_{1h}$. Without loss of generality, we assume that $\int_0^\infty s_h^2 \, d\tau < \int_0^\infty s_g^2 \, d\tau < \infty$. By using (65), we have

$$0 < \int_0^\infty (s_g^2 - s_h^2) d\tau = \int_0^\infty (\alpha_{1g}^2 - \alpha_{1h}^2) s_1^2 + 2(\alpha_{1g} - \alpha_{1h})\alpha_2 s_1 s_2 d\tau < \infty. \tag{68}$$

Then, it implies from (67) that

$$\int_0^\infty (s_g^2 - s_h^2) d\tau = \int_0^\infty -(\alpha_{1g} - \alpha_{1h})^2 s_1^2 d\tau + \int_0^\infty 2(\alpha_{1g} - \alpha_{1h}) s_1 s_g d\tau > 0. \tag{69}$$

Applying (65), we have

$$\int_0^\infty (\rho|s_g| + \lambda s_g^2) d\tau \le V(0) < \infty. \tag{70}$$

It follows from (70) that $\rho \int_0^\infty |s_g| d\tau < \infty$, which indicates $s_g \in L_1$. From (69), we obtain

$$\begin{aligned}&\int_0^\infty (\alpha_{1g}-\alpha_{1h})^2 s_1^2 d\tau\\ &< \int_0^\infty 2(\alpha_{1g}-\alpha_{1h}) s_1 s_g d\tau\\ &\le 2|\alpha_{1g}-\alpha_{1h}|\cdot ||s_1||_\infty \cdot ||s_g||_1 < \infty.\end{aligned} \tag{71}$$

Thus,

$$\int_0^\infty s_1^2 d\tau < \infty. \tag{72}$$

Similarly, we have

$$\int_0^\infty s_2^2 d\tau < \infty. \tag{73}$$

From the above analysis, we have $s_1 \in L_2 \cap L_\infty$, $\dot{s}_1 \in L_\infty$, $s_2 \in L_2 \cap L_\infty$, and $\dot{s}_2 \in L_\infty$. It follows from Barbalat's Lemma that

$$\lim_{t\to\infty} s_1 = 0, \quad \lim_{t\to\infty} s_2 = 0. \tag{74}$$

Note that $s_2 = c_3 e_4 + e_5 = c_3 x_3 + x_4$. As a result of $x_4 = \dot{x}_3$ in (13), it implies that we have $\lim_{t\to\infty} x_3 = 0$. According to (12), (38), and (41), the original system can be expressed as

$$\dot{E}_1 = AE_1 + E_2, \tag{75}$$

where

$$E_1 = [e_1, e_2]^T, \quad A = \begin{pmatrix} 0 & 1 \\ -c_1 & -c_2 \end{pmatrix}, \quad E_2 = [0, s_1 + \tilde{d}_w]^T.$$

Let $Q = Q^T > 0$, then it implies from A is Hurwitz that the Lyapunov equation $A^T P + PA = -Q$ has a unique solution $P = P^T > 0$. Choose the Lyapunov function candidate

$$V_1 = E_1^T P E_1. \tag{76}$$

The time derivative of V_1 can be given by

$$\begin{aligned}\dot{V}_1 &= \dot{E}_1^T P E_1 + E_1^T P \dot{E}_1\\ &= E_1^T (A^T P + PA) E_1 + 2E_1^T P E_2\\ &= -E_1^T Q E_1 + 2E_1^T P E_2\\ &\le -\lambda_{\min}(Q)||E_1||^2 + 2\lambda_{\max}(P)||E_2||\ \ ||E_1||,\end{aligned} \tag{77}$$

where $\lambda_{\min}$ and $\lambda_{\max}$ represent minimum and maximum eigenvalues, respectively. By virtue of (77), we have

$$\dot{V}_1 \le -\frac{1}{2}\lambda_{\min}(Q)||E_1||^2 - \frac{1}{2}\lambda_{\min}(Q)\left(||E_1|| - \frac{2\lambda_{\max}(P)}{\lambda_{\min}(Q)}||E_2||\right)^2 + \frac{2\lambda_{\max}^2(P)}{\lambda_{\min}(Q)}||E_2||^2. \tag{78}$$

It follows from $V_1 = E_1^T P E_1 \le \lambda_{\max}(P)||E_1||^2$ that

$$\dot{V}_1 \le -\kappa V_1 + \delta, \tag{79}$$

where

$$\kappa = \frac{\lambda_{\min}(Q)}{2\lambda_{\max}(P)},$$
$$\delta = \frac{2\lambda^2_{\max}(P)}{\lambda_{\min}(Q)}||E_2||^2.$$

Then, we have

$$V_1 \le V_1(0)e^{-\kappa t} + \frac{\delta(1-e^{-\kappa t})}{\kappa}. \tag{80}$$

Note that δ can converge to an arbitrarily small value from (20) and (74). It implies from (80) that e_1 and e_2 can converge to an arbitrarily small value by appropriately choosing the design parameters. In other words, it indicates that both x_1 and x_2 will converge to an arbitrarily small value. This proof is completed.

4 | SIMULATION STUDY

In this section, the proposed dynamic model is verified by using NREL 5-MW wind turbine model, and the developed disturbance observer-based hierarchical sliding mode controller is tested on both the design model and the NREL 5-MW wind turbine model within FAST code.

4.1 | NREL computer-aided engineering tools

The NREL FAST code is used to simulate the loads and the dynamic responses of the NREL wind turbine models. The NREL FAST code introduces the aerodynamics, structural (elastic) dynamics, hydrodynamics, control, and servo dynamics, which is primarily composed of InflowWind, HydroDyn, AeroDyn, ElastoDyn, ServoDyn, MoorDyn, and SubDyn modules. InflowWind is used to compute wind velocities with the help of the time series of wind speed vectors. ElastoDyn represents a structural-dynamic model that outputs displacements, velocities, accelerations, and reaction loads to AeroDyn and ServoDyn. ServoDyn involves control and actuator models. For structural control purposes, two independent single degree-of-freedom TMD systems are incorporated into the FAST code (i.e., FASTv8).[23] In this paper, the performance of the designed controller will be evaluated by using FAST (version 8).

4.2 | Model validation

To verify the proposed dynamic model for the floating offshore wind turbine, we let the design model (9)–(11) and the NREL 5-MW wind turbine model in FAST oscillate freely from an initial platform pitch angle of $5\pi/180$ rad, and other initial conditions are all set to be 0. For the design

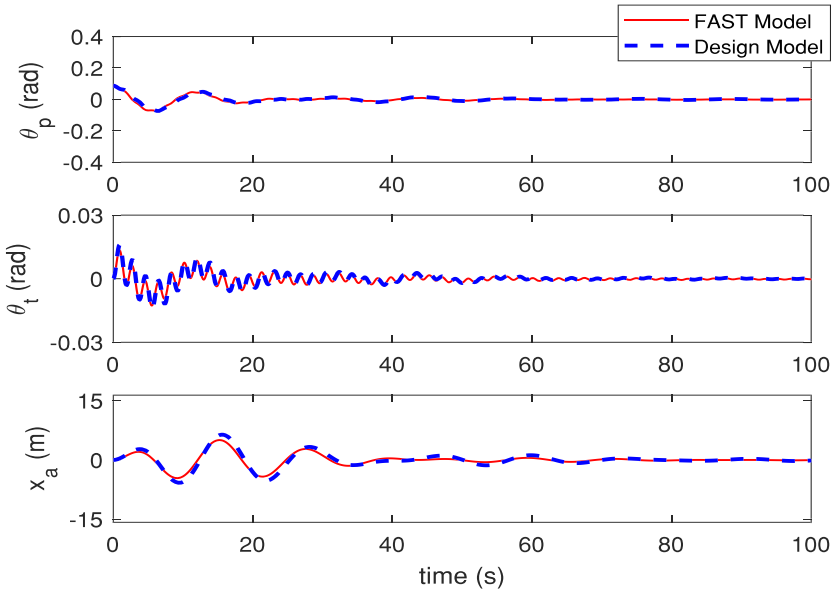

FIGURE 2 The response comparison between the design model given by (9)–(11) and the National Renewable Energy Laboratory 5-MW wind turbine model within the FAST code

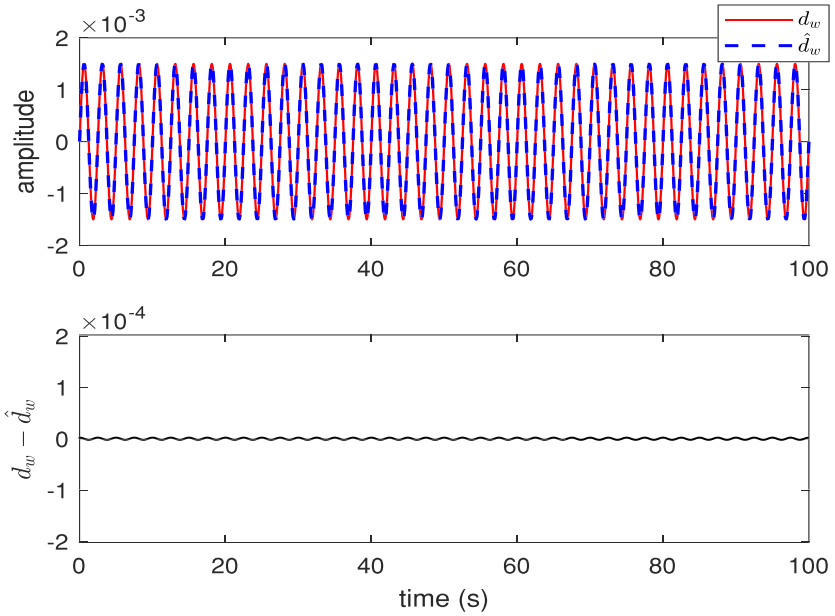

FIGURE 3 The estimation of the mismatched disturbances and the estimated errors

model, both M_w and F_a are set to be 0. Similarly, we disable the effects of both wind and wave for the NREL 5-MW wind turbine model. As shown in Figure 2, the simulation results of the platform pitch angles, the tower bending angles, and the TMD displacements in both models demonstrate a good match between them.

4.3 | Simulation results with the design model

In this section, the disturbance observer-based hierarchical sliding mode control architecture is implemented on the design model (12)–(14) in the presence of both the matched and mismatched disturbances. In the simulations, the initial conditions are given by $[x_1(0), x_2(0), x_3(0), x_4(0), x_5(0), x_6(0)] = [0.5\pi/180, 0, 0.8\pi/180, 0, 0, 0]$. The mismatched disturbance is described by $d_w = 0.0015\sin(0.8\pi t)$, and the matched disturbance is given by $d_z = 0.0012\sin(0.6\pi t)$. The design parameters of the controller is chosen as $c_1 = 36$, $c_2 = 12$, $c_3 = 40$, $\alpha_1 = 1$, $\alpha_2 = 80000$, $\lambda = 2$, $\beta_p = 1800$, $\beta_z = 1200$, $\epsilon_0 = 0.04$, $\epsilon_1 = 0.03$. The mismatched disturbance estimation results and estimated errors are plotted in Figure 3, and the matched disturbance estimation results and estimated errors are depicted in Figure 4. It implies from both Figures 3 and 4 that the excellent estimation accuracy

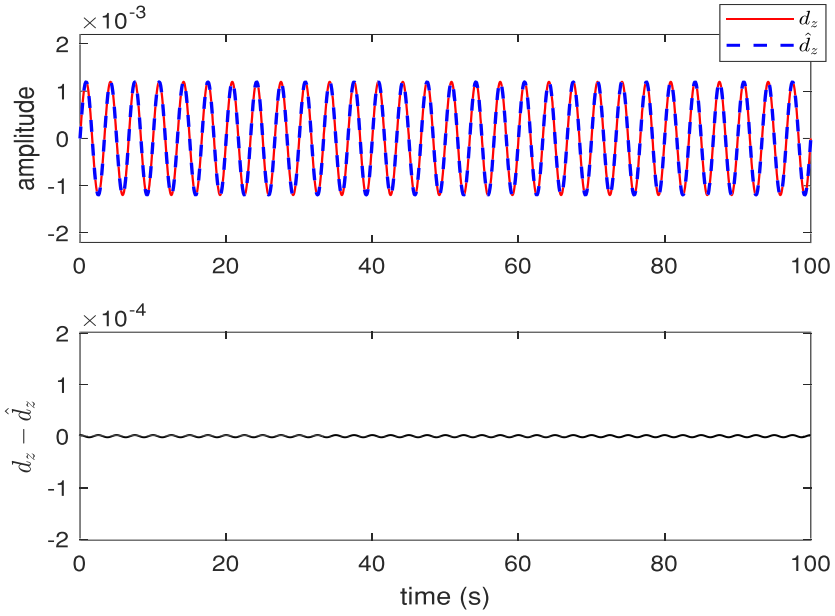

FIGURE 4 The estimation of the matched disturbances and the estimated errors

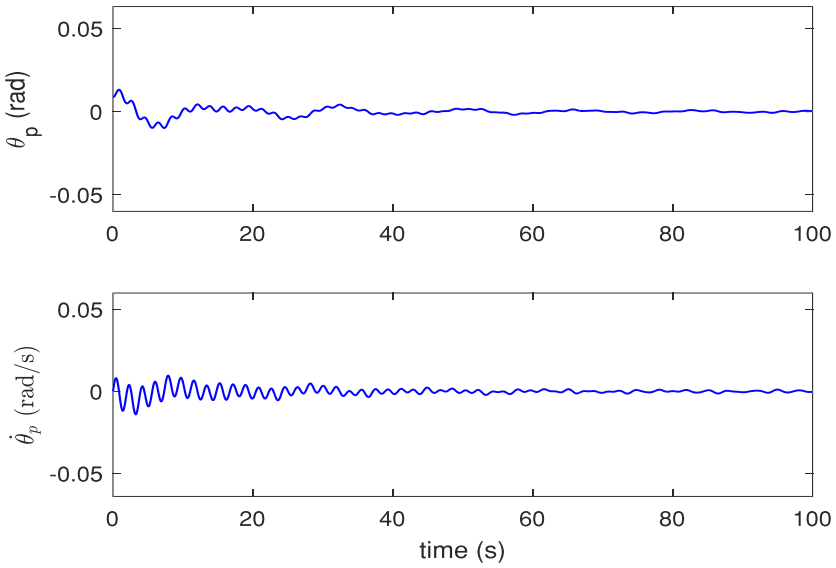

FIGURE 5 Platform pitch angle and velocity of the wind turbine

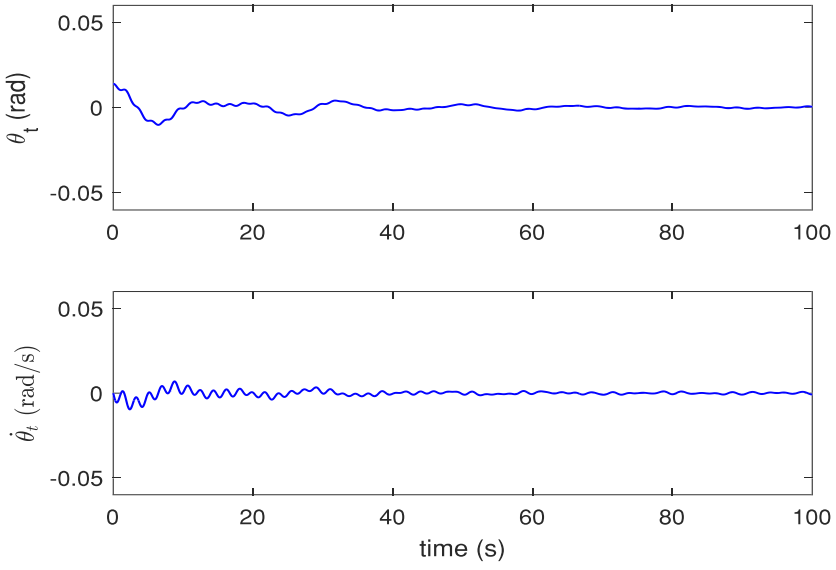

FIGURE 6 Tower bend angle and velocity of the wind turbine

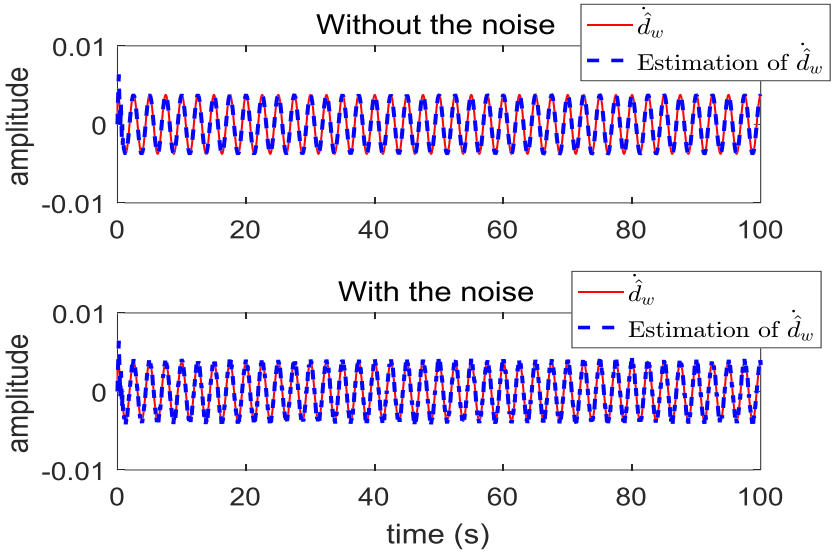

FIGURE 7 The estimations of $\dot{d}_w$ with and without the measurement noise under the sliding mode differentiator

is achieved with the proposed disturbance observer structures. The pitch angle displacement and velocity of the platform are provided in Figure 5, and the bend angle displacement and velocity of the tower are plotted in Figure 6. Figures 5 and 6 demonstrates that good control performances are achieved with the designed controller.

To evaluate the performance of the first-order sliding mode differentiator (47), the simulations are conducted with and without measurement noises, where the function randn is introduced to produce the measurement noises. The estimation results are plotted in Figure 7, and the estimated errors are shown in Figure 8. It indicates from Figure 8 that the estimated accuracy is degraded due to the adverse effect of the measurement noises.

In addition, multifrequency disturbances are also introduced in the simulations to further illustrate the advantage of the designed disturbance observers, where the mismatched disturbance and the matched disturbance are respectively described by

$$\begin{aligned} d_w = &\ 0.0002\sin(0.25\pi t) + 0.0004\sin(0.32\pi t) + 0.0006\sin(0.15\pi t), \\ d_z = &\ 0.0003\sin(0.16\pi t) + 0.0002\sin(0.10\pi t) + 0.0004\sin(0.24\pi t). \end{aligned}$$

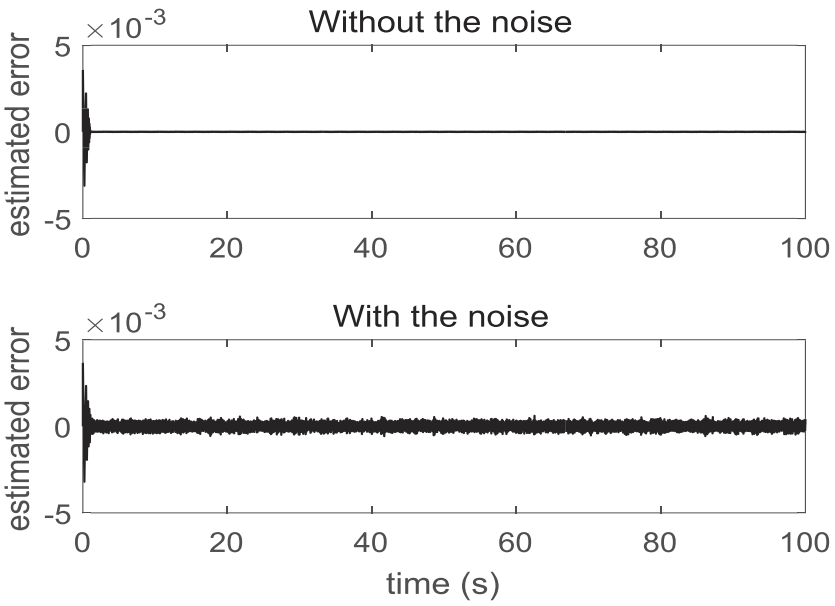

FIGURE 8 The estimated errors of $\dot{\hat{d}}_w$ with and without the measurement noise under the sliding mode differentiator

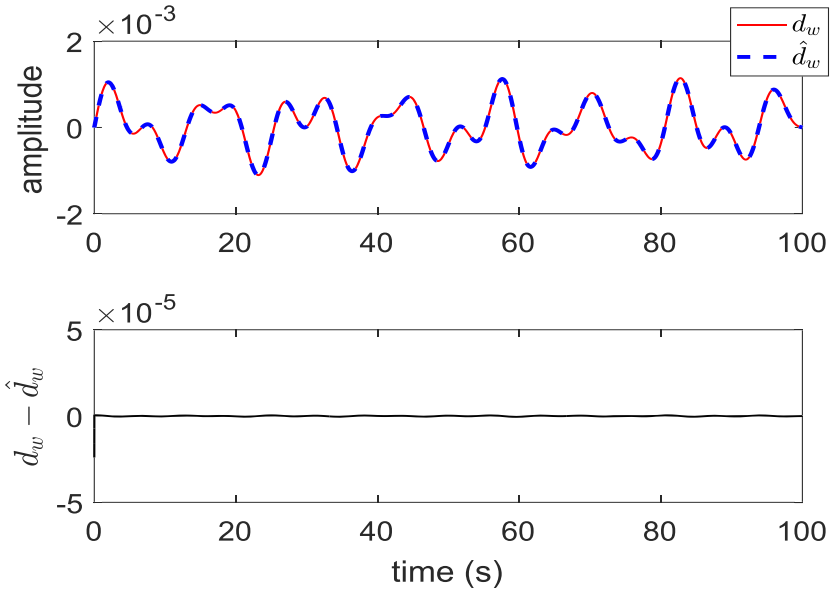

FIGURE 9 The estimation of the multifrequency mismatched disturbances and the estimated errors

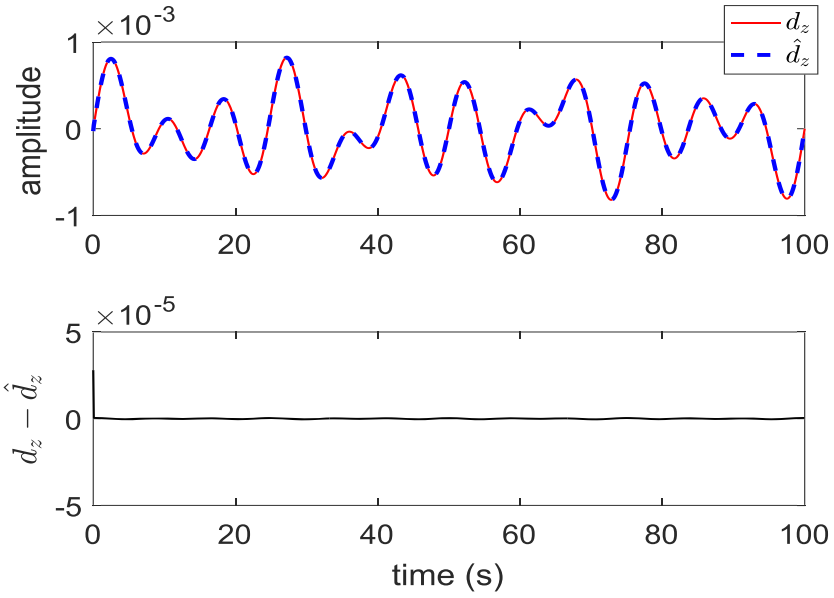

FIGURE 10 The estimation of the multifrequency matched disturbances and the estimated errors

The initial conditions are given by $\varepsilon_p(0) = 2.4 \times 10^{-5}$ and $\varepsilon_z(0) = -2.8 \times 10^{-5}$. The multifrequency disturbance estimation results are depicted in Figures 9 and 10. It implies from the disturbance estimation errors in Figures 9 and 10 that the developed disturbance observers can still maintain excellent estimation accuracy even if both the multifrequency disturbances and the initial errors are considered.

4.4 | Simulation results with the NREL 5-MW wind turbine model

To verify the active control performance, the proposed disturbance observer-based hierarchical sliding mode control algorithm is tested by the NREL 5-MW wind turbine model based on the FAST code, where the optimal parameters of the TMD are given by m_a = 400 000 kg, k_a = 103 019 N/m, and c_a = 60 393 N/(m/s).[12] The wind conditions in all the cases are generated based on the IEC Kaimal spectral model with normal turbulence model in TurbSim. The wave conditions in all the cases are generated by the HydroDyn module based on the JONSWAP spectrum. The peak-spectral period of the incident waves in all the cases is set to 10 s with the significant wave height being 5.5 m. In the first case, the mean hub-height longitudinal wind speed is 18 m/s (above-rated), and the turbulence intensity is Category A. The

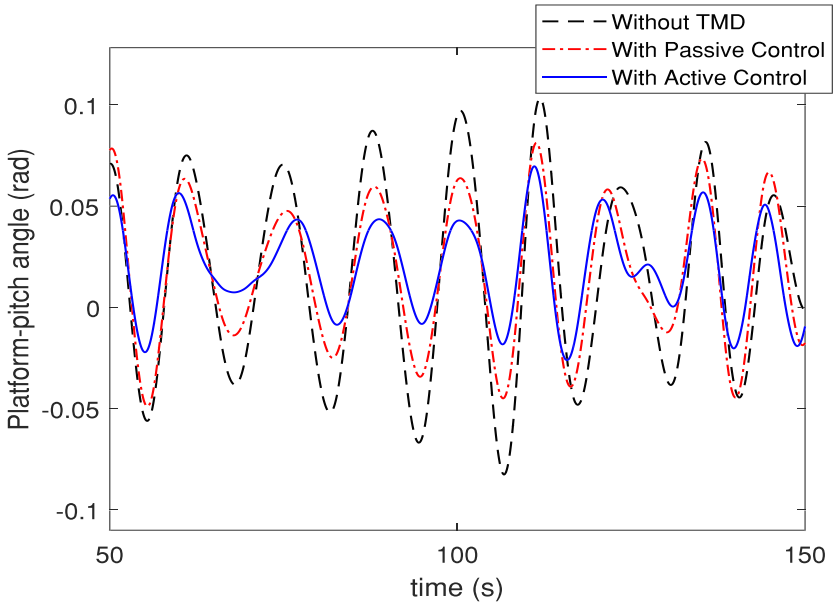

FIGURE 11 Time responses of the platform pitch angle with the mean hub-height longitudinal wind speed of 18 m/s. TMD, tuned mass damper

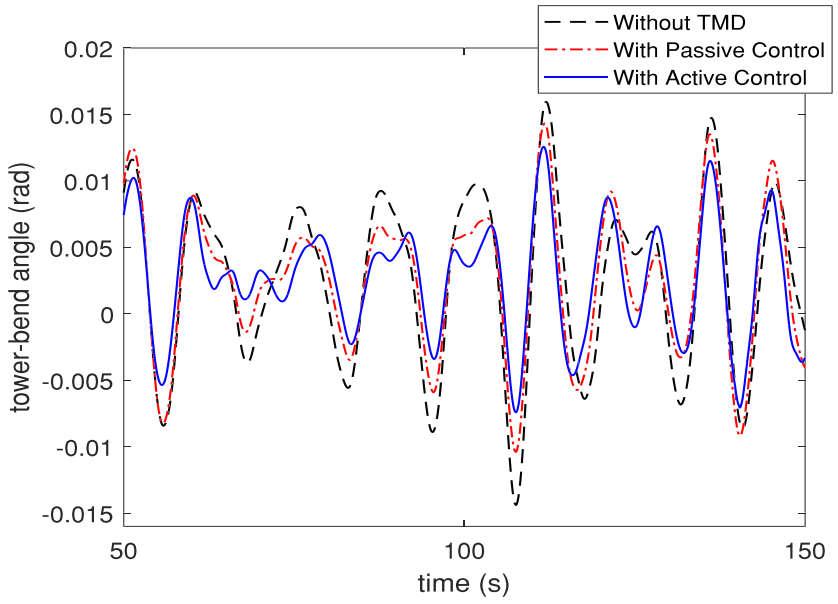

FIGURE 12 Time responses of the tower bend angle with the mean hub-height longitudinal wind speed of 18 m/s. TMD, tuned mass damper

time responses of the wind turbine with the proposed controller are shown in Figures 11 and 12 (for comparison purposes, both no TMD and passive control cases are considered), which shows that the proposed active controller has achieved significant improvement on the vibration suppression of the wind turbine compared with the passive control even if there exist model uncertainties and various disturbances such as winds and waves. To evaluate the energy consumption, it can be computed that the consumed average active TMD power accounts for 10% of the rated wind turbine power. A sensible design is that passive control works most of the time while the active control (basically adding an active force on top of the passive control) is activated only if the vibration is over certain limit. This can largely help reduce power consumption. To further validate the advantage of the proposed controller, the mean hub-height longitudinal wind speed of 24 m/s (above-rated) is chosen to conduct the simulation, and the turbulence intensity is Category B. As shown in Figures 13 and 14, the time responses of both the platform pitch angle and the tower bend angle are provided to demonstrate the vibration suppression performance. In this case, the average active energy consumption accounts for 12% of the rated wind turbine power. The simulation results without TMD and with passive control are plotted in Figures 13 and 14, which indicate that the great effectiveness and strong robustness of the proposed controller are achieved.

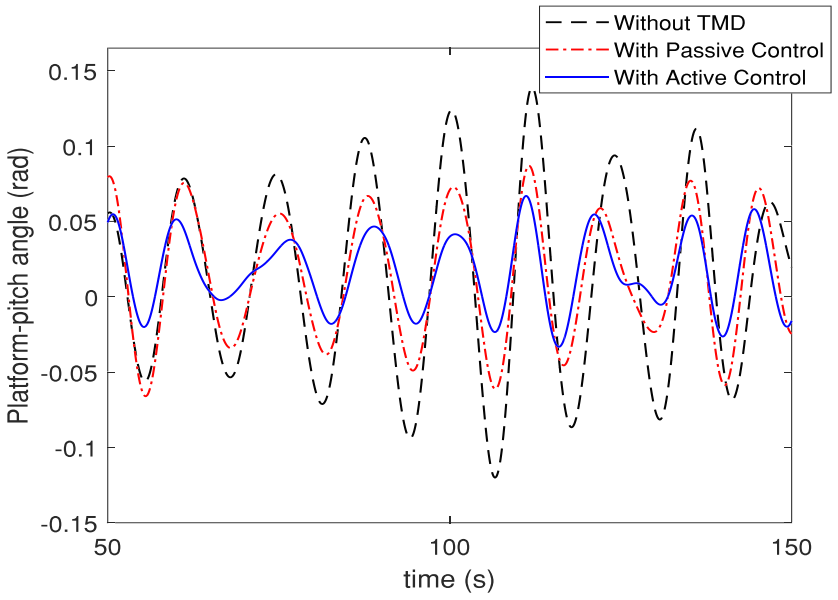

FIGURE 13 Time responses of the platform pitch angle with the mean hub-height longitudinal wind speed of 24m/s

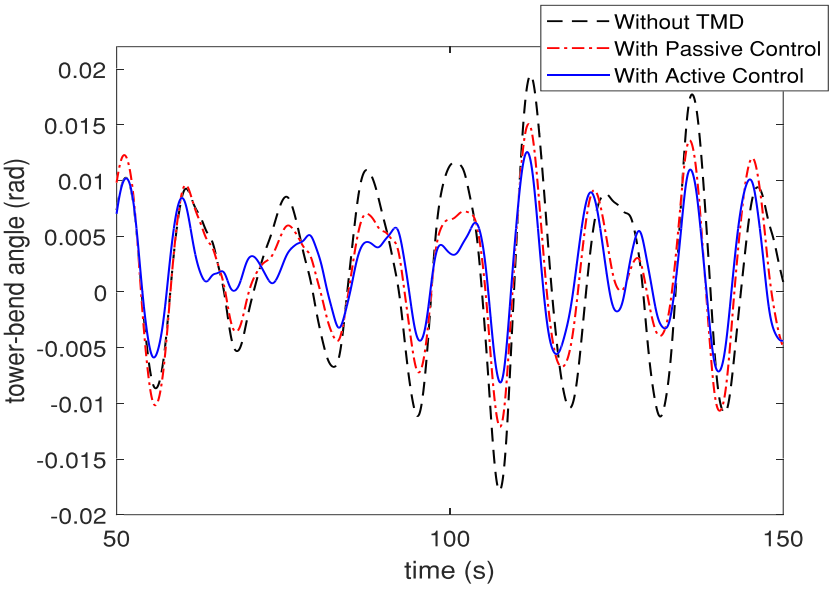

FIGURE 14 Time responses of the tower bend angle with the mean hub-height longitudinal wind speed of 24m/s

5 | CONCLUSION

In this paper, a nonlinear dynamic model for a TMD-based NREL 5-MW floating offshore wind turbine was derived. A disturbance observer-based hierarchical sliding mode control algorithm was proposed to stabilize such an underactuated nonlinear coupled system with both matched and mismatched disturbances. Two prescribed performance disturbance observers were independently constructed to estimate the matched and mismatched disturbances, and each estimation error can be adjusted by only one design parameter. With the disturbance observers, a hierarchical sliding mode controller was designed to suppress the vibration of the floating offshore wind turbine. Some sufficient conditions were derived to ensure the stability of the closed-loop system. The simulation results verified the accuracy of the developed design model and demonstrated the strong robustness and great effectiveness of the proposed control algorithm.

ORCID

Xiaowei Zhao https://orcid.org/0000-0002-1182-4502

REFERENCES

1. Wang Y, Hu Q, Srinivasan D, Wang Z. Wind power curve modeling and wind power forecasting with inconsistent data. *IEEE Trans Sustain Energy*. 2019;10(1):16-25.
2. Sun C, Jahangiri V. Bi-directonal vibration control of offshore wind turbines using a 3D pendulum tuned mass damper. *Mech Syst Sig Proc*. 2018;105:338-360.
3. Civelek Z, Luy M, Cam E, Mamur H. A new fuzzy logic proportional controller approach applied to individual pitch angle for wind turbine load mitigation. *Ren Energy*. 2017;111:708-717.
4. Stewart G, Lackner M. Offshore wind turbine load reduction employing optimal passive tuned mass damping systems. *IEEE Trans Cont Syst Tech*. 2013;21(4):1090-1104.
5. Hu Y, Wang J, Chen MZQ, Li Z, Sun Y. Load mitigation for a barge-type floating offshore wind turbine via inerter-based passive stuctural control. *Eng Struct*. 2018;177:198-209.
6. Yang J, He EM, Hu YQ. Dynamic modeling and vibration suppression for an offshore wind turbine with a tuned mass damper in floating platform. *Appl Ocean Res*. 2019;83:21-29.
7. Tong X, Zhao X, Karcanias A. Passive vibration control of an offshore floating hydrostatic wind turbine model. *Wind Energy*. 2018;21(9):697-714.
8. Sun C. Mitigation of offshore wind turbine responses under wind and wave loading: considering soil effects and damage. *Struct Cont Health Mon*. 2018;25(3):1-22.
9. Caterino N. Semi-active control of a wind turbine via magnetorheological dampers. *J Sound Vib*. 2015;345:1-17.
10. Pao LY, Johnson KE. Control of wind turbines. *IEEE Control Syst Mag*. 2011;31(2):44-62.
11. Lackner MA, Rotea MA. Structural control of floating wind turbines. *Mechatronics*. 2011a;21(4):704-719.
12. Li X, Gao H. Load mitigation for a floating wind turbine via generalized H_∞ structural control. *IEEE Trans Ind Electron*. 2016;63(1):332-342.
13. Li F, Wu L, Shi P, Lim CC. State estimation and sliding mode control for semi-Markovian jump systems with mismatched uncertainties. *Automatica*. 2015;51:385-393.
14. Park MS, Chwa D. Swing-up and stabilization control of inverted-pendulum systems via coupled sliding-mode control method. *IEEE Trans Ind Electron*. 2009;56(9):3541-3555.
15. Ashrafiuon H, Nersesov S, Clayton G. Trajectory tracking control of planar underactuated vehicles. *IEEE Trans Autom Control*. 2017;62(4):1959-1965.

16. Sankaranarayanan V, Mahindrakar AD. Control of a class of underactuated mechanical systems using sliding modes. *IEEE Trans Robot*. 2009;25(2):459-467.
17. Xu J, Wang M, Qiao L. Dynamical sliding mode control for the trajectory tracking of underactuated unmanned underwater vehicles. *Ocean Eng*. 2015;105:54-63.
18. Wang Z, Bao W, Li H. Second-order dynamic sliding-mode control for nonminimum phase underactuated hypersonic vehicles. *IEEE Trans Ind Electron*. 2017;64(4):3105-3112.
19. Wang W, Yi J, Zhao D, Liu D. Design of a stable sliding-mode controller for a class of second-order underactuated systems. *IEE Proc Cont Theory Appl*. 2004;151(6):683-690.
20. Yue M, Liu B. Adaptive control of an underactuated spherical robot with a dynamic stable equilibrium point using hierarchical sliding mode approach. *Int J Adapt Cont Sig Proc*. 2013;28(6):523-535.
21. Xu R, Ozguner U. Sliding mode control of a class of underactuated systems. *Automatica*. 2008;44(1):233-241.
22. Jonkman JM. Dynamics of offshore floating wind turbines-model development and verification. *Wind Energy*. 2009;12(5):459-492.
23. Lackner MA, Rotea MA. Passive structural control of offshore wind turbines. *Wind Energy*. 2011b;14(3):373-388.
24. Jonkman JM. *Dynamics Modeling and Loads Analysis of an Offshore Floating Wind Turbine*, National Renewable Energy Laboratory. USA: Golden, CO; 2007.
25. Chen M, Ge SS. Adaptive neural output feedback control of uncertain nonlinear systems with unknown hysteresis using disturbance observer. *IEEE Trans Ind Electron*. 2015;62(12):7706-7716.
26. Li Z, Su CY, Wang L, Chen Z, Chai T. Nonlinear disturbance observer-based control design for a robotic exoskeleton incorporating fuzzy approximation. *IEEE Trans Ind Electron*. 2015;62(9):5763-5775.
27. Shi C, Dong X, Xue J, Chen Y, Zhi J. Robust adaptive neural control for a class of non-affine nonlinear systems. *Neurocomputing*. 2017;223:118-128.
28. Yang J, Li S, Yu X. Sliding-mode control for systems with mismatched uncertainties via a disturbance observer. *IEEE Trans Ind Electron*. 2013;60(1):160-169.
29. Sun H, Li S, Yang J, Zheng WX. Global output regulation for strict-feedback nonlinear systems with mismatched nonvanishing disturbances. *Int J Robust Nonlinear Cont*. 2015;25(15):2631-2645.

How to cite this article: Zhang Y, Zhao X, Wei X. Robust structural control of an underactuated floating wind turbine. *Wind Energy*. 2020;1–20. https://doi.org/10.1002/we.2550